

24 agricultural field can reliably probe the water content of the top soil only if systematic effects due to the
25 biomass shielding are properly accounted for. Biomass corrected experimental values of soil water content
26 inferred from radiometric measurements are compared with gravimetric data acquired under different soil
27 moisture levels, resulting in an average percentage relative discrepancy of about 3% in bare soil condition and
28 of 4% during the vegetated period. The temporal evolution of corrected soil water content values exhibits a
29 dynamic range coherent with the soil hydraulic properties in terms of wilting point, field capacity and
30 saturation.

31 **Keywords**

32 Real-time continuous soil water content monitoring; precision agriculture; NaI gamma-ray spectra;
33 vegetation shielding effect; Monte Carlo simulation method; biomass equivalent water layer.

34 **1. Introduction**

35 Soil water content (SWC) is a relevant state variable tracking the exchange of water at the land
36 surface and is a key to understand and predict soil hydrological processes over a broad range of
37 scales (Vereecken et al., 2015). Tracing its dynamics provides essential information for a deeper understanding
38 of the major hydrological, biogeochemical, and energy exchange processes (Brocca et al., 2017), as well as
39 for improving water use efficiency in agriculture, which is definitely the main competitor in the worldwide
40 race to water resources (Levidow et al., 2014; Ozbahce and Tari, 2010). Therefore, technological and
41 methodological advancements are highly desired for accurate measurements of the spatial and temporal SWC
42 variability (Michot et al., 2003; Robinet et al., 2018; Sultana et al., 2017).

43 Recently, proximal and on-the-go soil sensors are being widely adopted for understanding soil
44 properties and hydrogeological processes in precision agriculture (Heggemann et al., 2017; Piikki et al., 2015;
45 Viscarra Rossel et al., 2007). From one side they have a relatively wider spatial coverage compared to point
46 scale sensors, and from the other side they are less subject to interfering factors (e.g. atmospheric effects or

47 observation conditions in terms of intensity and direction of illumination) in comparison to traditional remote
48 sensing methods based on satellite spectral images (Barnes et al., 2003; McBratney et al., 2003). In this
49 scenario, permanently installed measurement stations for proximal gamma-ray spectroscopy match the current
50 requirements for SWC sensing methods as they (i) keep the soil structure undisturbed during the data taking,
51 (ii) operate continuously allowing for a characterization of the SWC temporal dynamics and (iii) integrate
52 measurements at the field scale over areas of 1 to about 10 km² (Bogena et al., 2015; Strati et al., 2018).

53 Gamma-rays are high-energy photons continuously produced in soils due to the presence of ⁴⁰K and
54 daughter products of the ²³⁸U and ²³²Th decay chains. As the signal recorded by a spectrometer provides clues
55 on the propagation of gamma-rays from the emission to the detection point, environmental gamma spectra
56 probe at the same time the activity of the radioactive source and the physical-chemical properties of the
57 traversed materials in terms of different attenuation effects, the latter essentially dominated by material
58 density and consequently by SWC (Minty, 1997).

59 Environmental gamma-ray spectroscopy measurements are influenced by plenty of experimental
60 boundary conditions which knowledge help in interpreting radiometric data at different levels according also
61 to the spatial scale of the surveys. Airborne gamma-ray spectroscopy already raised the attention on the
62 attenuating effects on the gamma signal due to the presence of vegetation (Dierke and Werban, 2013;
63 Norwine et al., 1979; Sanderson et al., 2004; Wilford et al., 1997). However, the presence of biomass in terms
64 of plants, leaves and fruits is expected to play a much more critical role in proximal gamma-ray surveys,
65 which implies that an accurate estimate of the signal reduction is needed.

66 The physical-chemical properties and the radioactive content of agricultural soils can be considered
67 almost stationary, or at least sufficiently under control. The same does not apply to the crop system which is
68 subject to a highly dynamic development generally affected by variable climatic conditions and irrigation
69 management practices. Indeed, the presence of growing vegetation introduces a sizable extra attenuation due
70 to the Biomass Water Content (BWC). The BWC varies in time during the crop life-cycle and causes a

71 gamma-ray attenuation which is in principle undistinguishable from that generated by an increase in SWC. In
72 this perspective, a reliable correction for the BWC shielding is mandatory in order to avoid a systematic
73 overestimation of SWC.

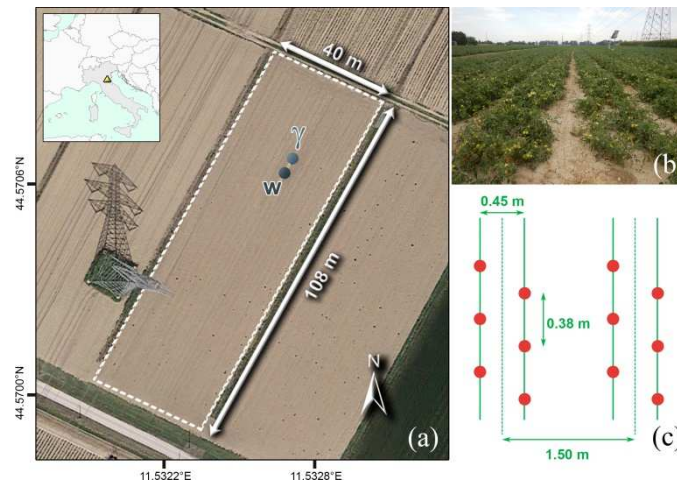
74 The goal of this paper is evaluating the BWC attenuation effect in the framework of a proximal
75 gamma-ray spectroscopy experiment performed at a tomato test field. The experiment was conducted by
76 installing a permanent gamma station constituted by a 1L sodium iodide (NaI) detector placed at a height of
77 2.25 m , which collected gamma-rays emitted within an area of about 25 m radial distance and within a depth
78 of approximately 30 cm. An ad-hoc gravimetric calibration campaign was performed by collecting soil and
79 biomass samples. Experimental daily values of the SWC were estimated over a data taking period that lasted
80 for 7 months and were evaluated by taking into account the shielding effect due to the presence of growing
81 BWC during the tomato crop season.

82 **2. Material and methods**

83 In the following section we briefly present a geographical and climatic setting of the experimental
84 site and a characterization of the main physical and hydraulic properties of the soil. The gamma and agro-
85 meteorological stations are described together with the data acquisition methods. The gravimetric sampling
86 campaign performed on soil and biomass samples is described along with the obtained results.

87 **2.1. Experimental site**

88 The experiment was conducted in the period 4th of April – 2nd of November 2017 at a tomato field of
89 the Acqua Campus, a research center of the Emiliano-Romagnolo Canal (CER) irrigation district in the Emilia
90 Romagna region in Italy (44.57° N, 11.53° E; 16 m above sea level) (Figure 1). According to the Köppen-
91 Geiger climate classification (Peel et al., 2007), this geographical area is classified as Cfa (i.e. temperate,
92 without dry season and with hot summer); its average annual temperature is 14 °C and rainfall is 700 mm.



93
 94 Figure 1. Panel (a), geographic location of the experimental site; the field dimensions and the positions of the gamma (γ) and agro-
 95 meteorological (w) stations are also reported (cartographic reference system WGS 84). Panel (b), picture of the tomato plants rows. Panel
 96 (c), schematic diagram of the disposition of the tomato plants rows.

97 About 24% of the agricultural territory in Emilia Romagna, one of the richest regions of Italy and
 98 Europe, is devoted to irrigated agriculture, which plays a major role in the regional economy (Munaretto and
 99 Battilani, 2014). In particular, Emilia Romagna is the Italian region having the largest surface of land
 100 cultivated with tomatoes, one of the most water-demanding crops among vegetables, and contributes for about
 101 one third of the tomato national production (ISTAT, 2017).

102 The main physical and hydraulic parameters of the soil, characterized by a loamy texture and a
 103 1.26% organic matter content, are listed in Table 1 (after (Strati et al., 2018)).

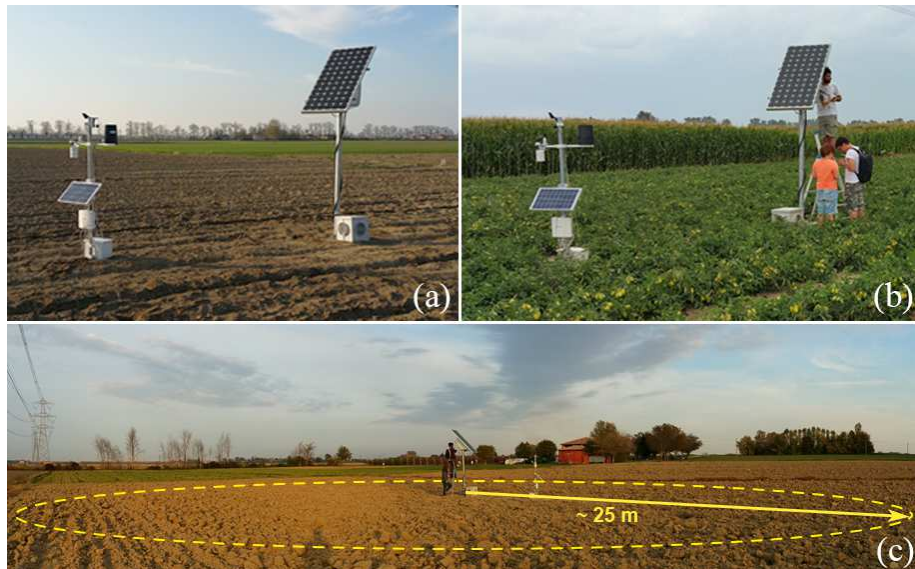
104 Table 1. Physical and hydraulic parameters of the experimental site soil for the depth horizon [0–30] cm, after (Strati et al., 2018). Sand,
 105 silt, and clay percentage as well as bulk density and organic matter were determined from direct measurements. The wilting point, field
 106 capacity and saturation value are inferred from the water retention curve.

Parameter	Value
Sand [%]	45
Silt [%]	40
Clay [%]	15
Soil textural class	Loam
Soil bulk density [kg/m ³]	1345
Wilting point (kg/kg)	0.07
Field capacity (kg/kg)	0.24
Saturation (kg/kg)	0.36

107 Tomato plants were transplanted on the 23rd of May with a row and plant spacing as shown in Figure
 108 1, which corresponds to a 3.5 plants/m² density, and harvested on the 14th of September. The crop
 109 phenological growth stages of anthesis and maturity, together with the planting and harvesting dates, are
 110 indicated in panel (a) of Figure 3. Irrigation water was delivered by a sprinkler system, following a schedule
 111 based on the criteria provided by the decision support tool of IRRINET (Munaretto and Battilani, 2014).

112 2.2. Experimental setup

113 The experimental setup is composed of a gamma spectroscopy station and a commercial agro-
 114 meteorological station (MeteoSense 2.0, Netsens) both powered by solar panels and provided with an internet
 115 connection (Figure 2).

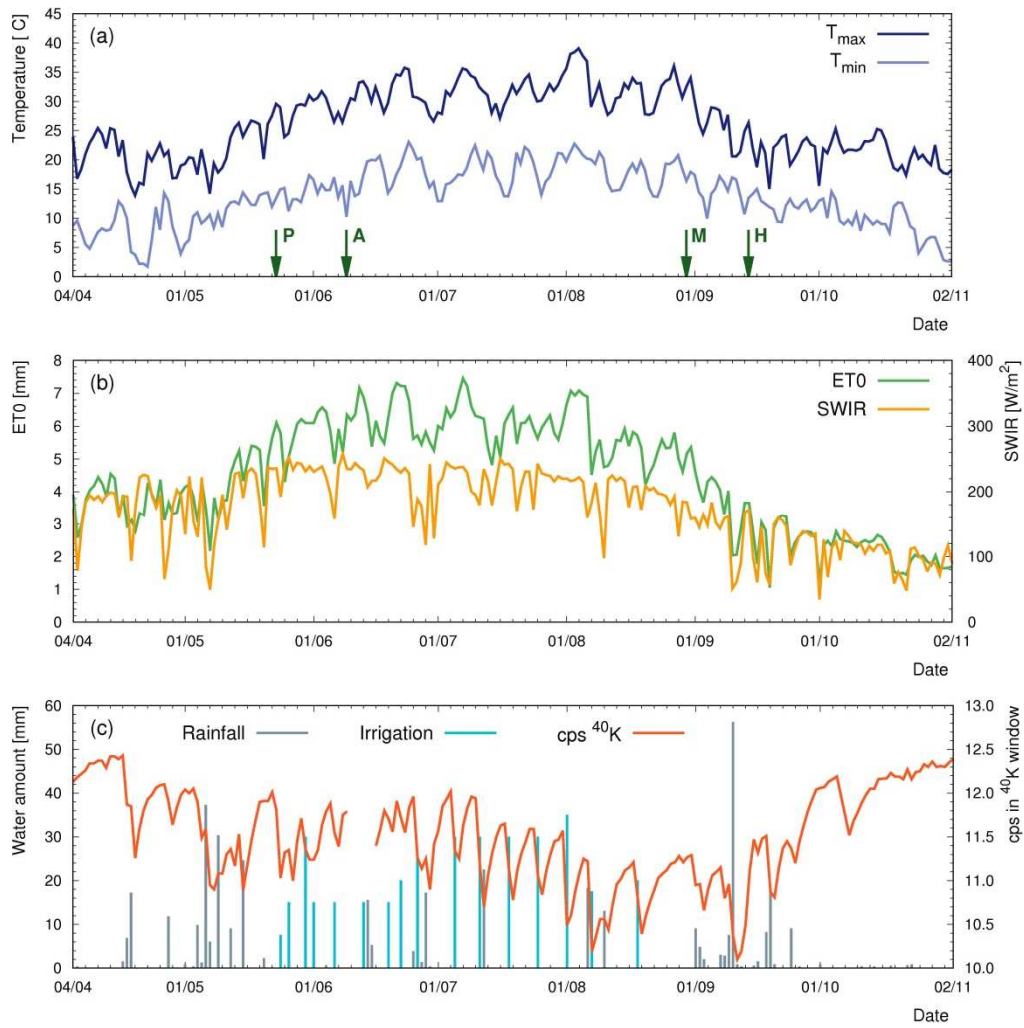


116
117 Figure 2. Panel (a) and (b) show the gamma and weather stations installed at the experimental site respectively in bare soil condition and
118 during the vegetated period. Panel (c) illustrates a schematic representation of the gamma-ray spectrometer footprint at 2.25 m height:
119 95% of the detected signal comes from an area having radius of ~25 m.

120 The gamma station was specifically designed and built for the purpose of this experiment: its
121 external structure is made up of steel and comprises a steel box welded on top of a 2.25 m high pole which
122 hosts a 1L sodium iodide (NaI(Tl)) gamma-ray spectrometer (Balducini et al., 2018). The crystal is coupled
123 to a photo-multiplier tube base which output is processed by a digital Multi-Channel Analyzer (MCA, CAEN
124 ystream) having 2048 acquisition channels. At a height of 2.25 m about 95% of the detected gamma signal is
125 produced within a cone having base radius of approximately 25 meters (Feng et al., 2009) (Figure 2).

126 The MCA is complemented with a small integrated computer which provides the necessary hardware
127 interface to the detector and runs the software required for managing the acquisition parameters, namely the
128 start time, the acquisition dynamics in terms of spectral gain [keV/ch], and the operating high voltage.
129 Additional software was developed to make the data-taking continuous and more resilient to some hardware
130 related failures like accidental restarts or power shortages.

131 Measured weather data include air temperature, relative air humidity, wind direction and speed,
132 precipitation and Short Wave Incoming Radiation (SWIR). Figure 3 shows the daily values of Minimum and
133 Maximum Temperatures (T_{\min} and T_{\max}), ranging in the $T_{\min} = [1.3 - 22.7]$ °C and $T_{\max} = [13.5 - 39.3]$ °C
134 intervals (panel a), the SWIR (ranging from 34.7 to 257.3 W/m²) (panel b), the daily rainfall amount (up to a
135 maximum of 56.2 mm) and irrigation water (up to a maximum of 35 mm) (panel c). The evapotranspiration
136 (ET₀, panel b) is calculated with the Hargreaves method (Hargreaves and Samani, 1985) using weather data
137 recorded by the agro-meteorological station. During the last ten years (2008 - 2017) local meteorological
138 archives (Arpae) recorded a mean total rainfall in the same period of 384.3 mm, a mean daily minimum
139 temperature of 13.2 °C and a mean daily maximum temperature of 26.3 °C.



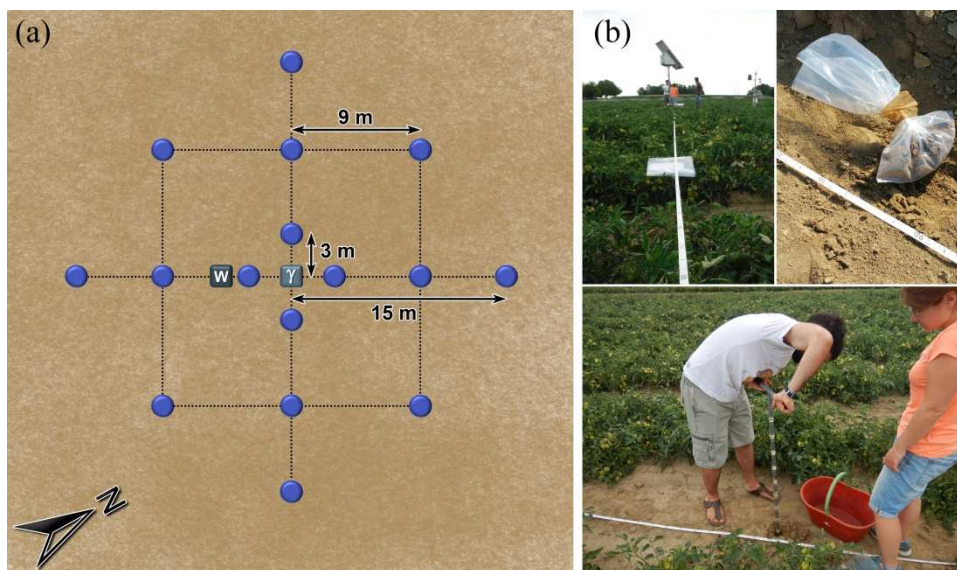
140
 141 Figure 3. Daily meteorological and gamma data. In panel (a), maximum (T_{\max}) and minimum (T_{\min}) temperatures; the arrows indicate
 142 crop stages of planting (P), anthesis (A), maturity (M) and harvesting (H). In panel (b), reference crop evapotranspiration (ET0) and Short
 143 Wave Incoming Radiation (SWIR). In panel (c), amount of rainfall and irrigation water and daily average counts per second (cps) in the
 144 ^{40}K gamma photopeak energy window.

145 2.3. Data acquisitions

146 2.3.1. Gravimetric measurements

147 Gravimetric measurements were carried out on bulk soil samples as means to both calibrate and
 148 validate the soil water content estimation based on proximal gamma-ray spectroscopy. Five sets of samples to
 149 be characterized via gravimetric measurements were collected: (i) a calibration set collected in bare soil
 150 condition on the 18th of September one day before a rainfall event, (ii) a validation set collected in bare soil
 151 condition on the 21st of September two days after a rainfall event, (iii) three validation sets collected in
 152 presence of the tomato crop and one Day Before Irrigation (DBI) (24th of July), one (26th of July) and three
 153 (28th of July) Days After Irrigation (DAI) (Table 2).

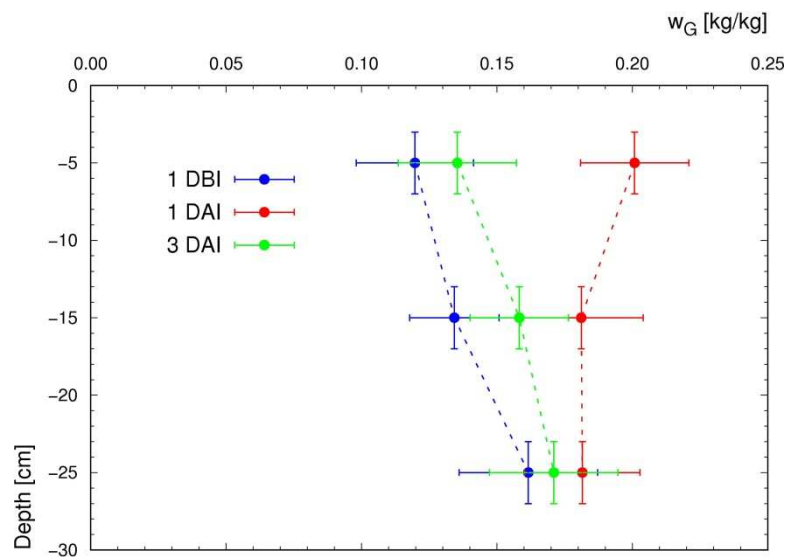
154 Samples were collected by using a soil-auger following a sampling scheme (Figure 4) including 16
 155 planar sampling points and covering homogeneously the area within a ~15 m radius from the gamma station
 156 position from which about 85% of the detected signal is produced (Figure 2 of (Baldoncini et al., 2018)).



157
 158 Figure 4. Panel (a), scheme of the 16 collection points adopted for the soil gravimetric sampling campaign together with their relative
 159 distances to the gamma (γ) and agro-meteorological (w) stations. Panel (b), different stages of the sampling procedure.

160 For each sampling planar position three samples were collected respectively in the [0 – 10] cm, [10 –
 161 20] cm and [20 – 30] cm depth horizons for a total number of 48 samples for each set. The gravimetric water
 162 content of each soil sample was evaluated after drying the samples at 105°C for about 24 h (Hillel, 1998).

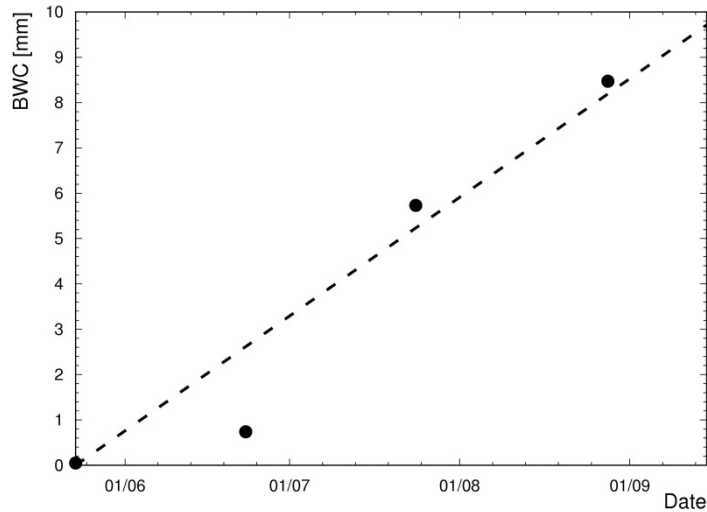
163 The results of the measurements (Figure 5) show a monotonically increasing trend in water content
 164 for increasing depth for the 1 DBI and 3 DAI depth profiles, which is reversed for the 1 DAI validation set.
 165 Among the three datasets the deepest soil horizon exhibits a much less pronounced variation in soil water
 166 content compared to the superficial layers.



167
 168 Figure 5. Individual gravimetric soil water contents (w_G) for the [0 – 10] cm, [10 – 20] cm and [20 – 30] cm depth horizons are reported
 169 in terms of mean and standard deviation of the corresponding 16 samples collected for the three sets of validation measurements
 170 performed in the vegetated period: 1 Day Before Irrigation (DBI) (24/07/17), 1 and 3 Days After Irrigation (DAI) (26/07/17 and
 171 28/07/17). Each data point is referred to the median depth, and the vertical error bar represents the 2 cm sampling uncertainty.

172 Above-ground crop biomass samples were collected by using the destructive sampling method
 173 (Catchpole and Wheeler, 1992) at four different maturity stages. The plants, including stems, leaves and
 174 fruits, were sampled in different days at the same diurnal time. The water mass of stems plus leaves and of
 175 fruits was separately evaluated by drying the samples at 80°C for about 24 h (SERAS, 1994) . For each

176 biomass gravimetric sampling campaign, the measured overall water mass per plant (kg/plant) was converted
 177 to BWC in mm by adopting the specific density of 3.5 plants/m². Data on BWC (mm) were linearly fitted to
 178 obtain the BWC temporal evolution over the vegetated period (Figure 6).



179
 180 Figure 6. Overall Biomass Water Content (BWC) in mm estimated from destructive gravimetric measurements on stems, leaves and fruits
 181 samples collected at four different maturity stages of the tomato crop. Data were fitted according to a linear regression curve with a 0.084
 182 mm/day slope and a 0.921 coefficient of determination.

183 2.3.2. Gamma-ray measurements

184 The gamma-ray spectrometer detects the photon radiation produced in the decays of natural
 185 occurring radionuclides (⁴⁰K, ²³⁸U and ²³²Th) and records a list mode output, i.e. a continuous logging of
 186 individual photons arrival time and acquisition channel. A dedicated software was developed to post-process
 187 the output list mode files in order to (i) generate gamma spectra corresponding to 15 minutes acquisition time,
 188 (ii) perform an energy calibration procedure, (iii) remove the spectral background, and (iv) retrieve the net
 189 count rate in the main ⁴⁰K, ²¹⁴Pb (²³⁸U) and ²⁰⁸Tl (²³²Th) photopeak energy windows (IAEA, 2003). Average
 190 net count rates are 11.51 cps in the ⁴⁰K energy window (1.37 – 1.57 MeV), 0.89 cps in the ²¹⁴Pb energy
 191 window (1.66 – 1.86 MeV) and 2.49 cps in the ²⁰⁸Tl energy window (2.41 – 2.81 MeV), while the gross

192 counting statistics in the [0.30 – 3.00] MeV range is of about 200 cps. While ^{40}K and ^{208}Tl are distributed only
193 in the soil, ^{214}Bi gamma radiation has an atmospheric component due to the exhaled ^{222}Rn gas which makes
194 the ^{214}Bi count rate inadequate for soil water content estimation as it clearly fluctuates in the day-time and in
195 relation to rainfall events (Barbosa et al., 2017). Given also the typically higher net counting statistics in the
196 main photopeak compared to ^{208}Tl , ^{40}K is chosen as natural gamma emitter for soil water content assessment
197 purposes.

198 Thanks to a specifically developed management software, gamma and meteorological data were
199 temporally aligned and merged in a unique database having a 15 minutes temporal resolution and 44 different
200 fields (34 related to gamma measurements and 10 to meteorological measurements). Data were hourly
201 averaged and a statistical fluctuation typically lower than 1% is observed in the net number of events. The
202 global dataset has 20502 entries corresponding to a 5125 hours acquisition time during which both the gamma
203 and agro-meteorological stations were operative, for a 260 GB total amount of raw data.

204 **3. Soil water content estimation**

205 **3.1. Theoretical background**

206 The inverse proportionality between soil moisture and gamma signal is the key point suggesting that
207 gamma-ray spectroscopy can be an operative method for retrieving SWC (Carroll, 1981; Grasty, 1997).
208 (Baldoncini et al., 2018) provides by means of Monte Carlo simulations a proof of concept of the
209 effectiveness and reliability of proximal gamma-ray spectroscopy for the determination of the gravimetric
210 SWC, w_G (kg/kg).

211 The SWC at time t can be determined by monitoring the counting statistics of a gamma spectrum in
212 the photopeak of energy E_i (Baldoncini et al., 2018) as:

213
$$w_{\gamma}^i(t) = \frac{S^{Cal}(E_i)}{S(E_i, t)} \cdot [\Omega(E_i) + w_G^{Cal}] - \Omega(E_i) \quad (1)$$

214 where

215 $S(E_i, t)$ (cps) is the net count rate in the photopeak of energy E_i at time t ,

216 $S^{Cal}(E_i)$ (cps) is the net count rate in the photopeak of energy E_i at the calibration time,

217 w_G^{Cal} (kg/kg) is the SWC determined on the basis of independent measurements at the calibration
218 time.

219 The adimensional factor $\Omega(E_i)$ is defined as:

220
$$\Omega(E_i) = \Psi(E_i) + [1 - \Psi(E_i)] \cdot f_{H_2O}^{struct} \quad (2)$$

221 where $f_{H_2O}^{struct}$ (kg/kg) is the fraction of structural water (i.e. water incorporated in the formation of soil
222 minerals) and $\Psi(E_i)$ corresponds to the ratio between the mass attenuation coefficient of the soil solid portion

223 $\left(\frac{\mu}{\rho}\right)_s$ (cm²/g) and the mass attenuation of water $\left(\frac{\mu}{\rho}\right)_{H_2O}$ (cm²/g):

224
$$\Psi(E_i) = \frac{\left(\frac{\mu}{\rho}(E_i)\right)_s}{\left(\frac{\mu}{\rho}(E_i)\right)_{H_2O}} \quad (3)$$

225 By adopting the specific values referred to the composition of the soil at the experimental site
226 (Baldoncini et al., 2018), Eq. (1) can be numerically written for the ⁴⁰K photopeak (1.46 MeV) as:

$$w_{\gamma K}(t) = \frac{S_K^{Cal}}{S_K(t)} \cdot [0.899 + w_G^{Cal}] - 0.899 \quad (4)$$

In absence of a detailed mineralogical analysis, a $\Omega = (0.903 \pm 0.011)$ mean value can be employed (Baldoncini et al., 2018). In any case, the uncertainty on the estimated SWC is typically dominated by the systematic uncertainty on the S_K^{Cal} and w_G^{Cal} calibration reference values, implying an almost negligible contribution from the Ω variability to the ~ 0.017 kg/kg absolute uncertainty.

In order to extract time-by-time SWC values from proximal gamma-ray spectroscopy measurements it is necessary to take into account a non-constant correction due to the presence of growing vegetation beneath the detector position (Figure 2). Indeed, as the tomato plants mature, the gamma spectrometer receives a progressively reduced gamma flux due to the shielding effect produced by the crop system. The latter can be estimated by modelling stems, leaves and fruits as an equivalent water layer characterized by a given thickness which we express as a BWC in units of mm (Figure 6). In particular, the time dependent correction to be applied to the measured gamma signal S can be expressed as the Λ ratio given in:

$$\Lambda_K(BWC) \left[\frac{cps}{cps} \right] = \frac{S_K^{MC}(BWC)}{S_K^{MC}(BWC=0)} \quad (5)$$

It follows that the SWC corrected for the attenuation due to the vegetation $w_{\gamma K}^\Lambda$ at time t is given by:

$$w_{\gamma K}^\Lambda(t) = \frac{S_K^{Cal} \cdot \Lambda_K(BWC(t))}{S_K(t)} \cdot [0.899 + w_G^{Cal}] - 0.899 \quad (6)$$

With the aim of going after the crop evolution temporal profile, a curve describing the attenuation factor $\Lambda(BWC)$ as function of the BWC was determined by adopting the Monte Carlo simulation method described in (Baldoncini et al., 2018) (Figure 7 panel a). Nine independent simulations were performed by

245 progressively increasing the thickness of the equivalent water layer from BWC = 0 mm up to BWC = 20 mm
 246 with steps of 2.5 mm. Simulations were carried out with an initial statistics of 10^9 emitted photons having
 247 1.46 MeV energy and assigning to the soil source a SWC corresponding to w_G^{Cal} . The nine $\Lambda(BWC)$ values
 248 were fitted according to a linear regression curve with an intercept fixed by definition to 1 (Figure 7 panel a).

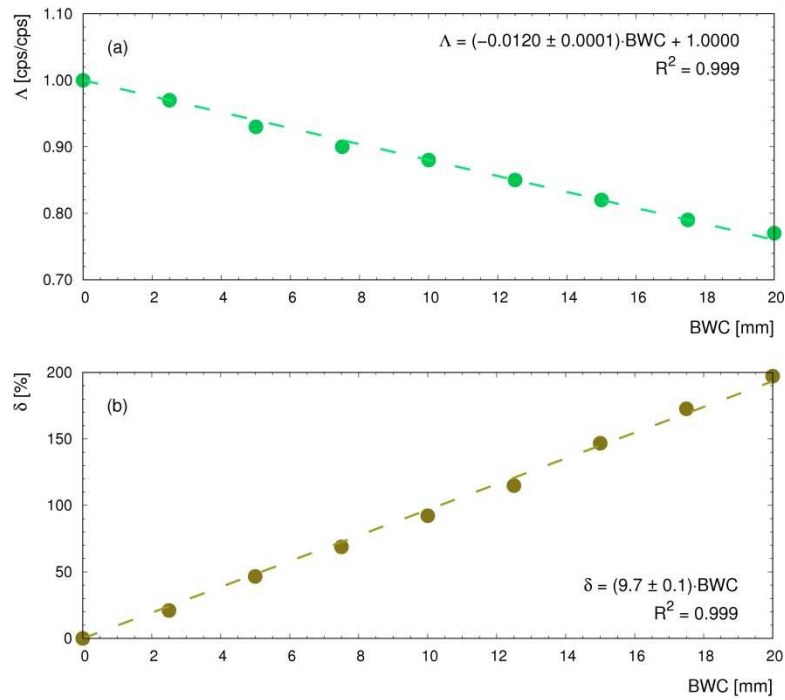
249 In order to estimate how the attenuation due to vegetation affects the estimation of SWC, we
 250 evaluate on the basis of the Monte Carlo results the quantity δ defined as:

$$251 \quad \delta(BWC)[\%] = 100 \cdot \frac{w'_{\gamma K} - w_G^{Cal}}{w_G^{Cal}} \quad (7)$$

252 where:

$$253 \quad w'_{\gamma K} = \frac{S_K^{Cal}}{S_K^{Cal} \cdot \Lambda(BWC)} \cdot [0.899 + w_G^{Cal}] - 0.899 = \frac{1}{\Lambda(BWC)} \cdot [0.899 + w_G^{Cal}] - 0.899 \quad (8)$$

254 that corresponds to the SWC that would have been measured without correcting for BWC for fixed w_G^{Cal} in the
 255 soil. As shown in Figure 7 panel b, the non-corrected SWC $w'_{\gamma K}$ differs from the $w_G^{Cal} = 0.163$ kg/kg
 256 calibration value (Table 2) by about 70% for a BWC of 7.5 mm, which almost corresponds to the estimated
 257 BWC at the tomato harvesting (Figure 6). Therefore, the non-application of a vegetation correction factor
 258 $\Lambda(BWC)$ to the measured gamma signal has a large systematic effect on the SWC estimation in proximal
 259 gamma-ray spectroscopy (Figure 8).



260
 261 Figure 7. Panel (a), simulated values of Λ (Eq. (5)) for the 1.46 MeV ^{40}K gamma emission energy as function of the BWC fitted with a
 262 linear regression curve. Panel (b), percentage overestimation δ (Eq. (7)) of the SWC as function of the BWC in case no vegetation cover
 263 correction is applied.

264 3.2. Experimental results and discussion

265 The theoretical approach presented in Section 3.1 was applied to the analysis of gamma-ray spectra
 266 measured over the entire data taking period; 54% of the data taking was carried out during the vegetated
 267 phase. As detailed in Section 2.3.1, a gravimetric sampling campaign was performed with the objective of
 268 both calibrating and validating the SWC estimation based on ^{40}K radiometric data (Table 2). The w_G values
 269 referred to [0–10] cm, [10–20] cm, and [20–30] cm were combined with weights respectively equal to 0.79,
 270 0.16, and 0.05, determined on the basis of the depth profile of the expected contribution to the overall gamma
 271 signal (Figure 5 of (Strati et al., 2018)). Particular attention was paid in collecting soil samples in different
 272 environmental conditions in terms of both temporal proximity to irrigation events and of biomass amount

273 present in the crop. This sampling strategy allowed for testing the reliability of the proximal gamma-ray
 274 spectroscopy method as well as for having insights on the bias that the BWC has on the SWC estimation.

275 Table 2. Results of SWC (w_G) for the gravimetric calibration measurement (18 September, one day before a rainfall event) and for four
 276 validation measurements. The latter were performed in bare soil condition (21 September, two days after a rainfall event) and during the
 277 vegetated period, one day before an irrigation event (24 July), one (26 July) and three days (28 July) after the same event. The w_G values
 278 are the weighted average SWC determined from 16 planar sampling points homogeneously distributed within 15 m from the gamma
 279 station. For each measurement we report the SWC inferred from proximal gamma-ray spectroscopy measurements without ($w_{\gamma K}$) and
 280 with BWC correction ($w_{\gamma K}^\Lambda$) together with the corresponding 1σ uncertainty. Δw and Δw^Λ are the percentage differences between w_G
 281 and $w_{\gamma K}$ and between w_G and $w_{\gamma K}^\Lambda$, respectively.

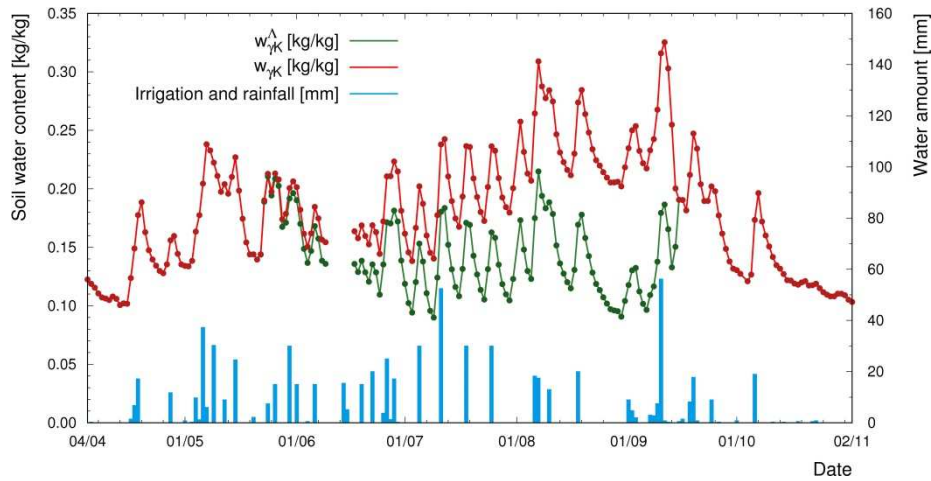
Date	w_G [kg/kg]	$w_{\gamma K}$ [kg/kg]	$w_{\gamma K}^\Lambda$ [kg/kg]	Δw [%]	Δw^Λ [%]
18 September	0.163 ± 0.008	0.163 ± 0.017	0.163 ± 0.017	0	0
21 September	0.176 ± 0.011	0.182 ± 0.017	0.182 ± 0.017	3	3
24 July	0.124 ± 0.021	0.196 ± 0.017	0.126 ± 0.017	58	2
26 July	0.197 ± 0.021	0.256 ± 0.017	0.181 ± 0.017	30	-8
28 July	0.141 ± 0.021	0.203 ± 0.017	0.133 ± 0.017	44	-6

282 For the validation measurement performed in bare soil condition (21st of September) the correction
 283 of BWC plays no role, as the value of the attenuation function Λ is identical to 1 for null BWC (see Eq. (5)).
 284 The three validation measurements performed on the 24th, 26th and 28th July allow for investigating the effect
 285 of the BWC correction as the tomato crop was at about midlife of its growing cycle. If the attenuation due to
 286 the presence of BWC is neglected, (see Eq. (4)), the $w_{\gamma K}$ would be affected by a systematic positive bias
 287 larger than 30%. By accounting for the attenuation effect of BWC (see Eq. (6)), an excellent agreement
 288 between $w_{\gamma K}^\Lambda$ and w_G is obtained, with a maximum relative discrepancy below 10% and a 1σ level agreement
 289 for all the three validation measurements. Therefore, systematic errors leading to underestimations or
 290 overestimation of the SWC are to be excluded also in presence of the tomato crop at the experimental site.

291 Considering that the BWC changes in time as the tomato crop grows, a non-constant BWC
292 correction was applied to gamma signals over the entire tomato life cycle. The temporal evolution of the
293 attenuation correction factor was estimated on the basis of the BWC temporal growth (see Figure 6).

294 Figure 8 shows a positive correlation between radiometric inferred SWC and the amount of
295 precipitations that includes both rainfall and irrigation water. Nevertheless, the $w_{\gamma K}^{\Lambda}$ and $w_{\gamma K}$ datasets exhibit
296 significantly different dynamic ranges. In order to have a meaningful interpretation of the SWC variation
297 domain it is necessary to account for the soil hydraulic properties, which are typically used as reference for
298 defining crop water demand. Indeed, the systematic bias obtained by neglecting the BWC correction can lead
299 to non-physical results corresponding to SWC frequently exceeding soil field capacity and sometimes
300 reaching values close to saturation (see Section 2.1), especially when the crop approaches the maturity stage
301 (Figure 8). During the vegetated period, $w_{\gamma K}^{\Lambda}$ values vary from 0.09 kg/kg to 0.21 kg/kg, coherently with the
302 range identified by wilting point (0.07 kg/kg) and field capacity (0.24 kg/kg). Conversely, the $w_{\gamma K}$ values vary
303 from 0.14 kg/kg to 0.33 kg/kg and show a substantial progressive positive drift as the tomato crop matures.

304 In the perspective of employing proximal gamma-ray spectroscopy for automatic irrigation management, the
305 BWC correction is mandatory for assessing crop water demand and for a sustainable use of water. The
306 method developed in this work for the assessment of the BWC shielding effect relies on the modelling of
307 biomass with equivalent water layers and is in principle independent from the type of crop sowed in the
308 agricultural field. Nonetheless, more field measurements over different vegetation types are desirable in order
309 to confirm the performance of the method, in particular for crops characterized by high water content or in the
310 case of tall trees cultivations.



311
 312 Figure 8. SWC inferred from measured ^{40}K count rate without ($w_{\gamma K}$, see Eq. (4)) and with ($w_{\gamma K}^{\wedge}$, see Eq. (6)) BWC correction for the
 313 entire data taking period.

314 4. Conclusions

315 The continuous tracing of soil water content provided by radiometric measurements has high
 316 potentialities for a site specific rational irrigation planning aimed at a sustainable use of water. In this study
 317 we demonstrate that proximal gamma-ray spectroscopy performed with permanent stations can be considered
 318 an effective tool for estimating soil water content for the following reasons: (i) the installation of a proximal
 319 gamma-ray spectroscopy station is economically affordable, (ii) the method is able to provide SWC time
 320 series with hourly frequency, sensitive to transient soil moisture levels and consistent with soil hydraulic
 321 properties, (iii) the method provides a continuous monitoring of SWC with a field scale footprint, filling the
 322 gap between punctual and satellite soil moisture measurement techniques, (iv) the results are affected by a
 323 ~10% relative uncertainty and are in agreement with independent validation gravimetric measurements on soil
 324 samples.

325 An unbiased quantitative estimate of the gravimetric water content requires a proper correction of the
 326 measured gamma signal for the reduction caused by water distributed in the growing vegetation.

327 We demonstrate that a reliable way to evaluate the shielding due to stems, leaves and fruits is to
328 model biomass as an equivalent water layer which thickness increases during the crop life-cycle. Monte Carlo
329 simulations highlight that gamma-ray measurements are not only extremely sensitive to water in the soil but
330 also to water concentrated in the biomass which acts as a shielding layer sitting on top of the soil gamma
331 source. In particular, the gamma signal is affected by a sizeable reduction on the order of 10% for 10 mm
332 equivalent water thickness, which would translate into a soil water content estimation biased by 90%.

333 Soil water content inferred from proximal gamma-ray spectroscopy was validated against
334 independent gravimetric measurements. The validation set of measurements performed in bare soil condition
335 provides an excellent result, with a 3% relative deviation of the gamma estimated value from the reference
336 gravimetric one. By applying the BWC correction to gamma measurements acquired during the vegetated
337 period, the systematic positive bias on SWC is prevented and an average relative discrepancy of 4% for the
338 validation measurements is observed. In closing, neglecting the BWC shielding effect would provide
339 overestimated soil water content values implying that proximal gamma-ray spectroscopy would be useless as
340 a monitoring and decision support tool for automatic irrigation scheduling, with negative impacts on crop
341 productivity.

342 **Acknowledgements**

343 This work was partially funded by the National Institute of Nuclear Physics (INFN) through the
344 ITALian RADioactivity project (ITALRAD) and by the Theoretical Astroparticle Physics (TAsP) research
345 network. The authors would like to acknowledge the support of the Project Agroalimentare Idrointelligente
346 CUP D92I16000030009, of the Geological and Seismic Survey of the Umbria Region (UMBRIARAD), of the
347 University of Ferrara (Fondo di Ateneo per la Ricerca scientifica FAR 2016) and of the MIUR (Ministero
348 dell'Istruzione, dell'Università e della Ricerca) under MIUR-PRIN-2012 project. The authors thank the staff
349 of GeoExplorer Impresa Sociale s.r.l. for their support and Renzo Valloni, Stefano Anconelli, Domenico

350 Solimando, Marco Bittelli, Vincenzo Guidi, Barbara Fabbri, Enrico Calore, Sebastiano Fabio Schifano,
351 Claudio Pagotto, Ivan Callegari, Gerti Xhixha and Merita Kaçeli Xhixha for their collaboration which made
352 possible the realization of this study. The authors show their gratitude to Giovanni Fiorentini, Miguel García
353 Castaño, Ilaria Marzola, Michele Montuschi and Barbara Ricci for useful comments and discussions. The
354 authors thank the Università degli Studi di Ferrara and INFN-Ferrara for the access to the COKA GPU
355 cluster.

356 **References**

- 357 Arpae, Agenzia regionale per la prevenzione, l'ambiente e l'energia dell'Emilia-Romagna. Dext3r, regional
358 meteorological database. <http://www.smr.arpa.emr.it/dext3r/> (accessed on 20 February 2018).
- 359 Baldoncini, M., Albéri, M., Bottardi, C., Chiarelli, E., Raptis, K.G.C., Strati, V., Mantovani, F., 2018.
360 Investigating the potentialities of Monte Carlo simulation for assessing soil water content via
361 proximal gamma-ray spectroscopy. *Journal of Environmental Radioactivity* 192, 105-116.
- 362 Barbosa, S.A., Miranda, P., Azevedo, E., 2017. Short-term variability of gamma radiation at the ARM Eastern
363 North Atlantic facility (Azores).
- 364 Barnes, E.M., Sudduth, K.A., Hummel, J.W., Lesch, S.M., Corwin, D.L., Yang, C., Daughtry, C.S., Bausch,
365 W.C., 2003. Remote-and ground-based sensor techniques to map soil properties. *Photogrammetric
366 Engineering & Remote Sensing* 69(6), 619-630.
- 367 Bogena, H.R., Huisman, J.A., Güntner, A., Hübner, C., Kusche, J., Jonard, F., Vey, S., Vereecken, H., 2015.
368 Emerging methods for noninvasive sensing of soil moisture dynamics from field to catchment scale:
369 A review. *Wiley Interdisciplinary Reviews: Water* 2(6), 635-647.
- 370 Brocca, L., Ciabatta, L., Massari, C., Camici, S., Tarpanelli, A., 2017. Soil moisture for hydrological
371 applications: Open questions and new opportunities. *Water* 9(2), 140.
- 372 Carroll, T.R., 1981. Airborne soil moisture measurement using natural terrestrial gamma radiation. *Soil
373 Science* 132(5), 358-366.
- 374 Catchpole, W., Wheeler, C., 1992. Estimating plant biomass: a review of techniques. *Austral Ecology* 17(2),
375 121-131.
- 376 Dierke, C., Werban, U., 2013. Relationships between gamma-ray data and soil properties at an agricultural
377 test site. *Geoderma* 199, 90-98.

- 378 Feng, T., Cheng, J., Jia, M., Wu, R., Feng, Y., Su, C., Chen, W., 2009. Relationship between soil bulk density
379 and PVR of in situ γ spectra. *Nuclear Instruments and Methods in Physics Research Section A: Accelerators, Spectrometers, Detectors and Associated Equipment* 608(1), 92-98.
- 380
381 Grasty, R.L., 1997. Radon emanation and soil moisture effects on airborne gamma-ray measurements.
382 *Geophysics* 62(5), 1379-1385.
- 383 Hargreaves, G.H., Samani, Z.A., 1985. Reference crop evapotranspiration from temperature. *Applied*
384 *engineering in agriculture* 1(2), 96-99.
- 385 Heggemann, T., Welp, G., Amelung, W., Angst, G., Franz, S.O., Koszinski, S., Schmidt, K., Pätzold, S.,
386 2017. Proximal gamma-ray spectrometry for site-independent in situ prediction of soil texture on ten
387 heterogeneous fields in Germany using support vector machines. *Soil and Tillage Research* 168, 99-
388 109.
- 389 Hillel, D., 1998. *Environmental soil physics: Fundamentals, applications, and environmental considerations*.
390 Elsevier, p.13.
- 391 IAEA, 2003. *Guidelines for radioelement mapping using gamma ray spectrometry data*. International Atomic
392 Energy Agency, Vienna. Technical Report Series No. 323.
- 393 ISTAT, 2017. Estimate of areas and production of agricultural cultivations.
394 [http://agri.istat.it/jsp/dawinci.jsp?q=plCPO0000010000023100&an=2017&ig=1&ct=418&id=15A|1](http://agri.istat.it/jsp/dawinci.jsp?q=plCPO0000010000023100&an=2017&ig=1&ct=418&id=15A|18A|69A|44A|28A)
395 [8A|69A|44A|28A](http://agri.istat.it/jsp/dawinci.jsp?q=plCPO0000010000023100&an=2017&ig=1&ct=418&id=15A|18A|69A|44A|28A) (accessed on 20 February 2018).
- 396 Levidow, L., Zaccaria, D., Maia, R., Vivas, E., Todorovic, M., Scardigno, A., 2014. Improving water-efficient
397 irrigation: Prospects and difficulties of innovative practices. *Agricultural Water Management* 146,
398 84-94.
- 399 McBratney, A.B., Santos, M.M., Minasny, B., 2003. On digital soil mapping. *Geoderma* 117(1-2), 3-52.
- 400 Michot, D., Benderitter, Y., Dorigny, A., Nicoullaud, B., King, D., Tabbagh, A., 2003. Spatial and temporal
401 monitoring of soil water content with an irrigated corn crop cover using surface electrical resistivity
402 tomography. *Water Resources Research* 39(5).
- 403 Minty, B.R.S., 1997. Fundamentals of airborne gamma-ray spectrometry. *AGSO Journal of Australian*
404 *Geology and Geophysics* 17, 39-50.
- 405 Munaretto, S., Battilani, A., 2014. Irrigation water governance in practice: the case of the Canale Emiliano
406 Romagnolo district, Italy. *Water Policy* 16(3), 578-594.
- 407 Norwine, J., Hansen, D., Saunders, D., Galbraith, J., 1979. Near-surface moisture and biomass influences on
408 the reliability of aerial radiometric surveys as a measure of natural radioelement concentrations,
409 Texas Instruments, Inc., Dallas (USA). Airborne Geophysical Services.

- 410 Ozbahce, A., Tari, A.F., 2010. Effects of different emitter space and water stress on yield and quality of
411 processing tomato under semi-arid climate conditions. *Agricultural Water Management* 97(9), 1405-
412 1410.
- 413 Peel, M.C., Finlayson, B.L., McMahon, T.A., 2007. Updated world map of the Köppen-Geiger climate
414 classification. *Hydrology and earth system sciences discussions* 4(2), 439-473.
- 415 Piikki, K., Wetterlind, J., Söderström, M., Stenberg, B., 2015. Three-dimensional digital soil mapping of
416 agricultural fields by integration of multiple proximal sensor data obtained from different sensing
417 methods. *Precision agriculture* 16(1), 29-45.
- 418 Robinet, J., von Hebel, C., Govers, G., van der Kruk, J., Minella, J.P., Schlesner, A., Ameijeiras-Mariño, Y.,
419 Vanderborght, J., 2018. Spatial variability of soil water content and soil electrical conductivity across
420 scales derived from Electromagnetic Induction and Time Domain Reflectometry. *Geoderma* 314,
421 160-174.
- 422 Sanderson, D., Cresswell, A., Hardeman, F., Debauche, A., 2004. An airborne gamma-ray spectrometry
423 survey of nuclear sites in Belgium. *Journal of environmental radioactivity* 72(1-2), 213-224.
- 424 SERAS, Scientific Engineering Response & Analytical Services, 1994. Standard operating procedures, plant
425 biomass determination. <https://clu-in.org/download/ert/2034-R00.pdf> (accessed on 6 March 2018).
- 426 Strati, V., Albéri, M., Anconelli, S., Baldoncini, M., Bittelli, M., Bottardi, C., Chiarelli, E., Fabbri, B., Guidi,
427 V., Raptis, K.G.C., 2018. Modelling Soil Water Content in a Tomato Field: Proximal Gamma Ray
428 Spectroscopy and Soil–Crop System Models. *Agriculture* 8(4), 60.
- 429 Sultana, S.N., mani Hazarika, U., Misra, U.K., 2017. Improvement of Water Use Efficiency and Remote
430 Sensing Applications for Surface Soil Moisture Monitoring. *ADB Journal of Engineering
431 Technology* 6(2).
- 432 Vereecken, H., Huisman, J.-A., Hendricks Franssen, H.-J., Brüggemann, N., Bogaen, H.R., Kollet, S., Javaux,
433 M., van der Kruk, J., Vanderborght, J., 2015. Soil hydrology: Recent methodological advances,
434 challenges, and perspectives. *Water resources research* 51(4), 2616-2633.
- 435 Viscarra Rossel, R., Taylor, H., McBratney, A., 2007. Multivariate calibration of hyperspectral γ - ray
436 energy spectra for proximal soil sensing. *European Journal of Soil Science* 58(1), 343-353.
- 437 Wilford, J., Bierwirth, P., e, Craig, M., 1997. Application of airborne gamma-ray spectrometry in soil/regolith
438 mapping and applied geomorphology. *AGSO Journal of Australian Geology and Geophysics* 17(2),
439 201-216.